TRANSACTIONS OF THE INSTITUTE OF AVIATION
No. 4 (245), pp. 7-15, Warsaw 2016
DOI: 10.5604/05096669.1226344

ISSN 0509-6669
eISSN 2300-5408

DEPENDENCE OF THE DAMAGE AREA ON IMPACT ENERGY IN FILAMENT-WOUND COMPOSITE TUBES

Marcelina Bobrowska*, Michał Barcikowski**

*Center for Composite Technologies, Institute of Aviation, Al. Krakowska 110/114, 02-256 Warsaw, Poland
** Department of Mechanics, Materials Science and Engineering, Faculty of Mechanical Engineering, Wroclaw University of Technology, ul. M. Smoluchowskiego 25, 50-370 Wrocław, Poland
marcelina.bobrowska@ilot.edu.pl, michal.barcikowski@pwr.edu.pl

Abstract

The research presented in this paper sought to characterize the relationship between the extent of delamination and impact energy in filament-wound composite structures. The subjects of the research were five-layered composite tubes that have been designed using the matrix method. This method was used to select three different mosaic patterns with different rest of the winding stroke parameters and number of interlaces. The interlaces are stress concentration locations and affect the strength of the composite. The tubes were manufactured using E-glass fiber roving reinforcement and epoxy resin. The composite filament-wound structures were subjected to a high velocity impact from a 2.0 g spherical hardened steel impactor propelled to a velocity of 140 - 170 m/s using a gas gun. Linear dependence of the damage area to the impact energy on filament-wound composite tubes, found in a previous study for polyester-matrix glass fibre-reinforced laminates, could be confirmed for only one material in this study.
Keywords: Filament-wound composite structures, impact damage, ballistic impact, filament winding.

1. INTRODUCTION

Increasingly wide usage of extremely stressed and simultaneously light constructions contributed to the intensive development of composites. Composite pressure vessels and composite filament-wound pipes, both made using filament winding - which consists in winding continuous fiber roving onto a rotating mandrel in predetermined patterns - are of this type of construction [1]. Application area of mentioned constructions requires effective methods of their structural health monitoring [2].

Mosaic patterns, applied in filament winding, are selected using an array method, and is also used in designing composite pressure vessels. This method, devised by Wojciech Błażejewski, allows the designer to obtain several types of weaves – mosaic patterns with a different sequence of bundle placements. The number of crossovers, strongly associated with the mentioned sequence, was the main criterion for pattern selection [3].

The impact energy is commonly provided using a gas gun, which may be capable of exercising both sub-ballistic (intermediate-velocity between 10 and 100 m/s) and ballistic impact. The sub-ballistic impact is especially common in aviation. The time of impact is short, so that elastic waves (both longitudinal and transverse) propagating in the material are not able to reach the edge of the

impacted object during the stroke [4]. High-velocity impact, also called ballistic impact, is characterized by a velocity of several hundred m/s. The duration – much shorter than the sub-ballistic impact is too short for elastic waves to propagate a significant distance through the material. The damage is confined to a small area around the impact point [5].

The damage mechanism as well as the material response to impact are complex and depend on many factors such as: impact velocity, angle of impact, impactor geometry and its mass, and shape and mass of the impacted object. The most important factor influencing damage mechanisms and accompanying phenomena is the impact velocity (not impact energy, as two impacts with the same energy but within different velocity regimes will produce different damages) [6].

Kinetic energy of the displaced part of the target object, fiber tension, fiber failure (either through tensile failure or shearing), delamination, matrix cracking, friction between the impactor and target material, and impactor deformation are most frequently cited modes of energy absorption and damage mechanism [7].

Research on impact resistance of composite structures made using filament winding has been, to date, concerned with low-velocity impacts [8, 9]. Thus, comparison between results presented in this paper (concerning ballistic impact damage) and results from the literature (concerning low-velocity impacts) is impossible.

In the study devoted to laminated composites, it was shown that the area delaminated as a result of an impact is directly proportional to the impact energy and no vertical offset is expected nor found. Moreover, reinforcement in the form of a continuous-filament mat compares favourably to loose woven roving; such reinforced composites have a much smaller area of delamination after impact for a given energy. The damage, as seen in the cross-section, is also less severe in continuous-filament mat-reinforced composites [10].

2. MOSAIC PATTERNS SELECTION

The Array Method allows composite structure designers to generate several types of weaves – mosaic patterns, with the objective to obtain a regular layer. Many parameters are used to describe this wound structure. The most important geometric parameter is the winding angle α, which is directly related to stress distribution in pressure vessels.

Tab. 1. Calculated parameters used to generate array for 13 tows [Author, 2015]

Calculated parameters	e = 5 mm	e = 17 mm
Tow width, $e_x = \frac{e}{\cos\alpha}$, mm	8.65	29.42
Number of tow, $Z = \frac{2\pi r}{e_x}$, mm	40	12
Winding lead, $s = \frac{\pi d}{\tan\alpha}$, mm	244.68	244.68
Cover rate, $C\% = \frac{Z \cdot e_x}{\pi d} \cdot 100\%$	100.15	102.21
Cover rate, $C\% = \frac{(Z+1) \cdot e_x}{\pi d} \cdot 100\%$	102.66	110.67

Using simple graphical-analytical techniques, the presented method describes the complicated filament-wound structure using two parameters - the winding angle α and the core diameter d. Thereby, it is possible to designate the following parameters: winding lead s and coefficient a being the rest of winding lead, selected from range $a \in (0, 1)$.

The mosaic pattern condition is fulfilled only when the core is completely covered with a uniform layer of saturated roving beams. Otherwise, gaps and inequalities occur. Proper selection of the mosaic pattern involves determining the optimal distribution of crossovers that become the sites of stress concentration and fracture initiators [11].

The average thickness of wound structures was set to approx. 4 mm. The calculated number of layers required for the winding corresponded to 11. Winding parameters were established as starting point for the necessary calculations: tow width – 5 and 17 mm, winding angle $\alpha = 54.7°$, core diameter $d = 110$ mm (constant over the entire length) (tab. 1).

The number of tows Z was increased by 1 and amounted 13 and 41 tows respectively, so that for the last wound layer of the cover ratio was at least 100 %. In addition, the odd number of tows ensures an almost 100 % cover rate.

Calculated parameters were used to generate an array for 13 tows (fig. 2). For the study, the following three mosaic patterns were chosen: N_r1, N_r2, and N_r4 with the least, the largest and intermediate number of crossovers respectively.

Fig. 1 displays the scheme of an exemplar N_r1 mosaic pattern from matrix 13 with highlighted characteristic sites. For each matrix with a natural number N_r1 mosaic pattern exists.

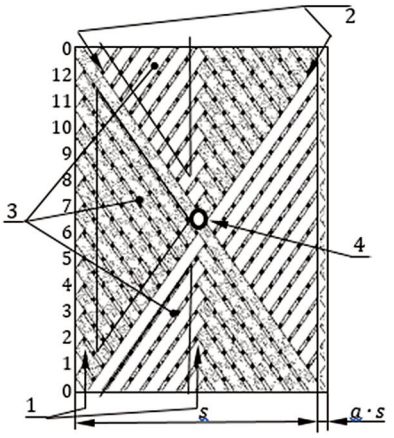

Fig. 1. N_r1 mosaic pattern scheme with characteristic areas: 1 – crossover lines (circumferential band), 2 – fiber undulation line (helical band), 3 – areas without crossovers (undulations), 4 – central point, s – winding lead, a – coefficient [Author, 2015]

N_r	πd													a
0	0	-	-	-	-	-	-	-	-	-	-	-	1	*0*
1	**0**	**1**	**2**	**3**	**4**	**5**	**6**	**7**	**8**	**9**	**10**	**11**	**12**	**13**	*1/26*
2	**0**	**7**	**1**	**8**	**2**	**9**	**3**	**10**	**4**	**11**	**5**	**12**	**6**	**13**	*2/26*
3	0	9	5	1	10	6	2	11	7	3	12	8	4	13	*3/26*
4	**0**	**10**	**7**	**4**	**1**	**11**	**8**	**5**	**2**	**12**	**9**	**6**	**3**	**13**	*4/26*
5	0	8	3	11	6	1	9	4	12	7	2	10	5	13	*5/26*
6	0	11	9	7	5	3	1	12	10	8	6	4	2	13	*6/26*
7	0	2	4	6	8	10	12	1	3	5	7	9	11	13	*7/26*
8	0	5	10	2	7	12	4	9	1	6	11	3	8	13	*8/26*
9	0	3	6	9	12	2	5	8	11	1	4	7	10	13	*9/26*
10	0	4	8	12	3	7	11	2	6	10	1	5	9	13	*10/26*
11	0	6	12	5	11	4	10	3	9	2	8	1	7	13	*11/26*
12	0	12	11	10	9	8	7	6	5	4	3	2	1	13	*12/26*
13	0	-	-	-	-	-	-	-	-	-	-	-	-	1	*13/26*
14	0	1	2	3	4	5	6	7	8	9	10	11	12	13	*14/26*
15	0	7	1	8	2	9	3	10	4	11	5	12	6	13	*15/26*
16	0	9	5	1	10	6	2	11	7	3	12	8	4	13	*16/26*
17	0	10	7	4	1	11	8	5	2	12	9	6	3	13	*17/26*
18	0	8	3	11	6	1	9	4	12	7	2	10	5	13	*18/26*
19	0	11	9	7	5	3	1	12	10	8	6	4	2	13	*19/26*
20	0	2	4	6	8	10	12	1	3	5	7	9	11	13	*20/26*
21	0	5	10	2	7	12	4	9	1	6	11	3	8	13	*21/26*
22	0	3	6	9	12	2	5	8	11	1	4	7	10	13	*22/26*
23	0	4	8	12	3	7	11	2	6	10	1	5	9	13	*23/26*
24	0	6	12	5	11	4	10	3	9	2	8	1	7	13	*24/26*
25	0	12	11	10	9	8	7	6	5	4	3	2	1	13	*25/26*
26	0	-	-	-	-	-	-	-	-	-	-	-	-	1	*26/26*

Fig. 2. „Table 13" (13 circumference bundles), N_r – type of layer, πd – bundles order on the circumference, value of a – rest of winding lead coefficient, $a \in (0, 1)$ [Author, 2015]

3. MATERIALS USED TO MADE FILAMENT-WOUND COMPOSITE TUBES

All samples for this research were prepared using E-glass fiber roving reinforcement ER 3005/1200/10. The diameter of the filament is 10 ÷ 15 microns. The roving is soft, mostly used as reinforcement for epoxy resins in filament winding or pultrusion.

Epoxy resin Epolam 5015 with hardener Epolam 2016 produced by Axson was the composition used to manufacture all of the tested composites. The materials were mixed in a weight ratio 100/36. Advantages of the applied mixture are variable reactivity, very good wettability of the fibers, no foaming and resistance to moist environments. Moreover, this combination of resin and hardener allows long duration winding, which is important in laboratory conditions, especially in winding thin beams.

The prepared samples were kept at 20°C for 24 hours and then cured at 70°C for 12 hours in accordance with the manufacturer's technical sheet.

Five composite tubes, with a length of 1000 mm, were manufactured. Average thickness of each sample and other characteristic parameters are shown in table 2.

Views of the actual structures and their graphic illustrations are shown in figure 3.

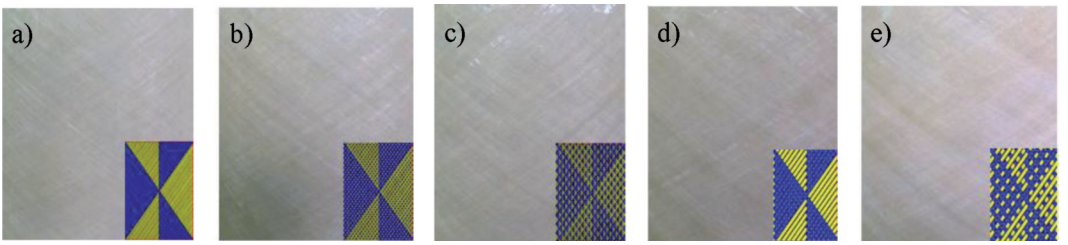

Fig. 3. Views of the actual structures and their graphic illustrations: a – N_r1 (5 mm); b – N_r2 (5 mm); c – N_r4 (5 mm); d – N_r1 (17 mm); e – N_r2 (17 mm) [Author, 2015]

Tab. 2. Parameters of manufactured structures [Author, 2015]

Mosaic pattern	Structure number (according to array table)	Tow width *e*, mm	Number of crossovers	Sample thickness, mm
N_r1	1	5	360	4.20
N_r2	2	5	3360	4.34
N_r4	4	5	2480	3.60
N_r1	1	17	96	5.84
N_r2	2	17	336	6.31

4. IMPACT TESTING

The composite tubes were subjected to ballistic impact using a compressed-air gun test assembly (fig. 4). The gas gun propels an impactor in the form of hardened steel ball 7.86 mm in diameter and 2.0 g in weight, by means of compressed air stored in a tank. The velocity of the free-flying impactor was measured by a ballistic chronograph (fig. 5b).

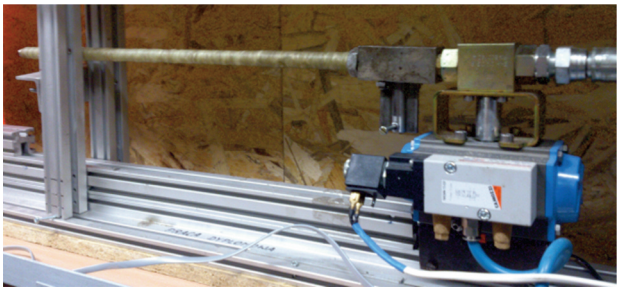

Fig. 4. Propelling part – gas gun [Author, 2015]

A specimen holder (fig. 5a) designed for test purposes enables the precise vertical and horizontal positioning of the specimen so that the impactor strikes normal to the lateral surface of the cylinder. Specimens were fixed to the specimen holder using two flexible bands.

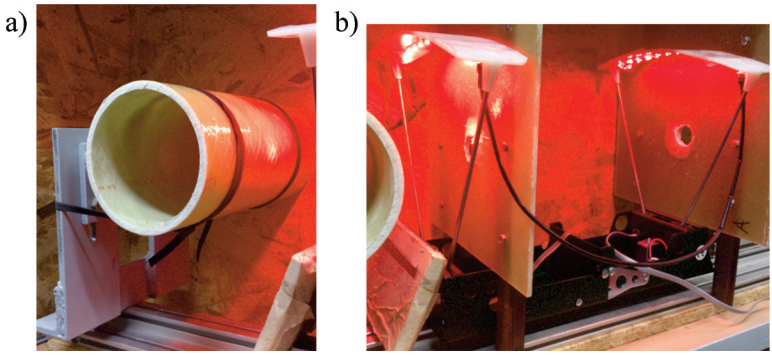

Fig. 5. Fixing and measuring part: a – specimen holder; b – measuring assembly [Author, 2015]

Each specimen was subjected to ballistic impact four times, rotating the specimen by 90° after each impact. The first point always corresponded to crossovers of the fibers in the last layer.

The tests encompassed velocities in the range of 144 ÷ 172 m/s, resulting in impact energies in the range of 21 ÷ 30 J (tab. 3).

Tab. 3. Velocity and kinetic energy of the impactor [Author, 2015]

Impactor velocity, m/s	Impactor energy, J
143,7 ± 1,2	20,65 ± 0,35
159,5 ± 1,2	25,43 ± 0,37
172,4 ± 1,3	29,71 ± 0,45

5. MEASUREMENT OF THE DAMAGE AREA AS VISIBLE IN TRANSMITTED LIGHT

Fig. 6 presents damage areas after an impact of 30 J, visible in daylight. The pine-tree shaped delamination interfaces increase through the thickness of the laminate, resulting in a front face delamination area smaller than the back face delamination area [12].

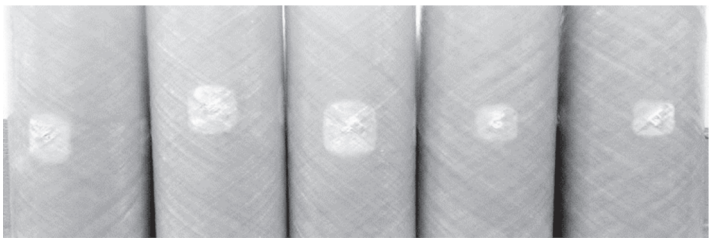

Fig. 6. Damage areas after impact 30 J, visible in daylight [Author, 2015]

The extent of delamination was evaluated by means of digital image analysis. Because the specimens were not flat, it was necessary to trace outlines of the damage areas on a carbon paper

pressed to cylindrical surfaces of the specimens. The obtained copies were scanned and resulting images were processed using Scion Image software to measure the contrasting delaminated area.

Transmitted light images of selected specimens after impact (damage visible) are presented in figure 7.

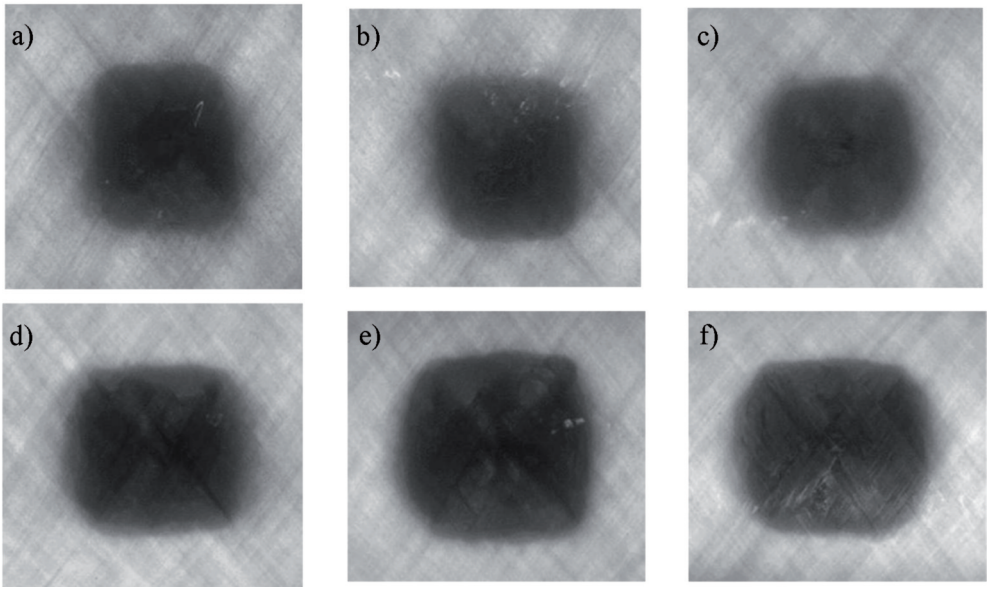

Fig. 7. Transmitted light images of specimens after impact: a – 20 J, N_r1 (17 mm); b – 25 J, N_r1 (17 mm); c – 30 J, N_r1 (17 mm); d – 20 J, N_r4 (5 mm); e – 25 J, N_r4 (5 mm); f – 30 J, N_r4 (5 mm) [Author, 2015]

Table 4 presents results of delamination damage for each material. The average damage area was calculated separately for points 1 and 3, which are places of fibers crossing last wound layer, and 2 and 4, being central points of a rhombus outlined by crossing fibers. It was expected that for filament-wound structures impact point affects the extent of delamination.

Tab. 4. Averaged results of delamination damage of the tested materials [Author, 2015]

Level of compressed air pressure		2 MPa			4 MPa			9 MPa		
Number of mosaic pattern		Impact velocity, m/s	Impact energy, J	Delamination area, mm^2	Impact velocity, m/s	Impact energy, J	Delamination area, mm^2	Impact velocity, m/s	Impact energy, J	Delamination area, mm^2
N_r1 (5 mm)	Point 1 and 3	143.7	20.7	1627.21	159.5	25.4	1885.58	172.4	29.7	1958.23
	Point 2 and 4			1648.61			1987.30			2001.03
N_r2 (5 mm)	Point 1 and 3			1660.24			2164.24			2245.08
	Point 2 and 4			1586.22			2315.39			2147.28
N_r4 (5 mm)	Point 1 and 3			1818.74			2112.17			2585.15
	Point 2 and 4			1986.48			2186.22			2470.55
N_r1 (17 mm)	Point 1 and 3			1339.33			1464.77			1550.32
	Point 2 and 4			1426.09			1471.02			1894.49
N_r2 (17 mm)	Point 1 and 3			1292.17			1242.49			1640.21
	Point 2 and 4			1245.80			1241.14			1521.27

As presented in figure 8, observed dependence of the damage area on impact energy was not strictly linear. Only for mosaic pattern N_r4 was the dependence found to be close to linear. It is important to remember that sample thicknesses were significantly different from each other. The specimen wound to mosaic pattern (N_r4) was the thinnest, which could be the explanation for the most extensive area of delamination observed in this study. Conversely, structure N_r2 with a 17 mm fiber width was the thickest, and the delamination area after impact for this specimen was the smallest.

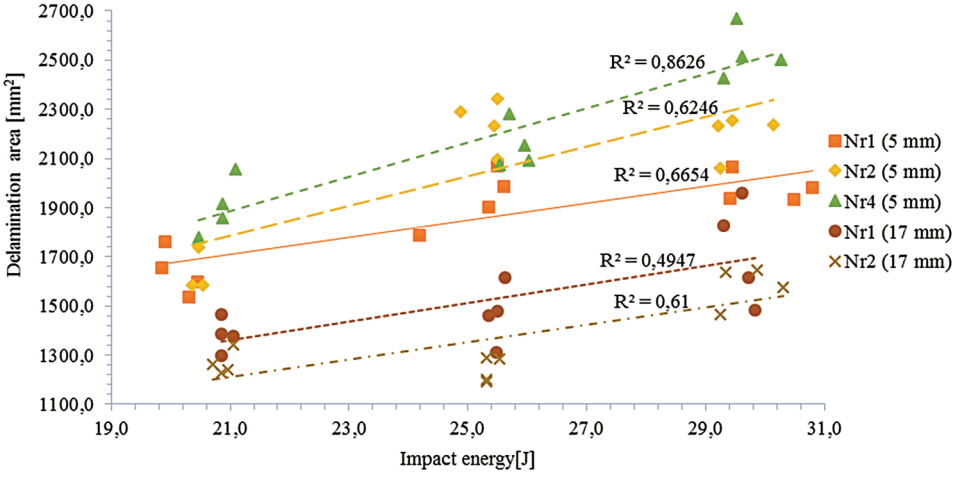

Fig. 8. Dependence of the delamination area on impact energy [Author, 2015]

6. CONCLUSIONS

Research presented in literature is concerned with low-velocity impact, and cannot be compared to the high-velocity impact results from this study. Observation of the impact damage surface allowed the authors to draw the following conclusions:

Presented study showed impact damage area increases in the range of 1194 ÷ 2670 mm^2 with an increasing impact velocity (144 ÷ 172 m/s). This dependence was observed for all studied mosaic patterns, independent of the number of crossovers.

Thickness of the specimen is negatively correlated to growth of delamination area with a rising impact velocity. This relation is clearly visible in specimen wound according to mosaic pattern N_r4. The most intensive increase on the X axis was noticed for mosaic pattern N_r4. Coefficient a (the slope) from the linear equation $y=ax+b$ corresponded to 70 and was twice higher as the others (except N_r2 (5 mm) for which the coefficient corresponded to 60). Observed growth of area of delamination for mosaic pattern N_r4 was doubled compared to the growth for other structures.

Linear dependence of delamination area on impact energy, expected according to literature related to low-velocity impact, was confirmed only for structure N_r4, where linear correlation coefficient was 0.8626 and coefficients calculated individually for different points of impact were close to 1.

Influence of each subsequent impact on the total strength of tested tube were not observed. All delamination areas resulting from impact were similar for all impact points of each tube. The variance between impact damage area for the 1 and 4 impact point was in the range of - 230 to + 280 mm^2 (minus means impact damage area for impact point number 4 was smaller than for point 1 and plus respectively inversely).

The filament winding process is not perfect. Small fiber displacement, incomplete fiber wetting, as well as possibility of air pockets between layers adversely affect the strength of the composite. Impacting at one of these points could influence the results.

Manually tracing the delamination area introduced a possibility of mistakes with a size of about 2 mm resulting from the subjective view of the researcher. Damaged surfaces were measured using the simplest way, i.e. by their manual tracing and then digital analysis. While the risk of error is small for the digitizing (the user is tasked only with selecting fields to be analyzed), the first part – manual tracing – is always fraught with human eye error.

There is an opportunity to improve the research by more accurate impact placement, or through devising another method (eg. a scanner) to accurately measure damaged surfaces, both of which would lead to a better understanding of the mechanisms of impact damage on filament wound composite tubes.

BIBLIOGRAPHY

[1] Królikowski W., 2012, *Polimerowe kompozyty konstrukcyjne*, Wydawnictwo Naukowe PWN, Warszawa.

[2] Nowosielska K., Kowalczyk P., 2008, Wykrywanie, lokalizacja i identyfikacja uszkodzeń w wysokowytrzymałych konstrukcjach kompozytowych, Prace Instytutu Lotnictwa, pp. 83-111.

[3] Błażejewski W., 2013, *Kompozytowe zbiorniki wysokociśnieniowe wzmocnione włóknami według wzorów mozaikowych*, Oficyna Wydawnicza Politechniki Wrocławskiej, Wrocław.

[4] Barcikowski M., 2012, Wpływ materiałów i struktury laminatów poliestrowo-szklanych na ich odporność na udar balistyczny, Praca doktorska ZUT, Szczecin.

[5] Cantwell W.J. and Morton J., 1991, "The impact resistance of composite materials – a review", Composites, **22**(5), pp. 347-362.

[6] Abrate S., 1998, Impact on composite structures, Cambridge University Press, New York, ISBN 0-521-47389-6 (hc).

[7] Naik N.K. and Shrirao. P., 2004," Composite structures under ballistic impact", Composite Structures, 66, pp. 579-590

[8] Matemilola S. A. and Stronge W. J., 1997, Low-Speed Impact Damage in Filament-Wound CFRP Composite Pressure Vessels, J. Pressure Vessel Technol, **119**(4), pp. 435-443.

[9] Alderson K.L.and Evans K.E., 1992, "Low velocity transverse impact of filament-wound pipes: Part 1. Damage due to static and impact loads", Composite Structures, Volume 20, Issue 1, pp. 37-45.

[10] Barcikowski M.i Semczyszyn B., 2011, "Impact damage in polyester-matrix glass fibre-reinforced composites", Part I, Impact damage extent, Kompozyty, **11**(3), pp. 230-234.

[11] Błażejewski W., 1999, „Wpływ struktury nawijania włókna na wytrzymałość elementów walcowych wykonanych z kompozytu epoksydowo-szklanego", Praca doktorska PWr, Wrocław.

[12] Minak G., Abrate S., Ghelli D., Panciroli R. and Zucchelli A., 2010, "Residual torsional strength after impact of CFRP tubes", Composites: Part B 41, pp. 637-645.

ZALEŻNOŚĆ PÓL USZKODZEŃ OD ENERGII UDARU RUR KOMPOZYTOWYCH WYTWORZONYCH METODĄ NAWIJANIA WŁÓKNA NA MOKRO

Streszczenie

Wyniki badań prezentowane w niniejszym artykule stanowią charakterystykę zależności pól uszkodzeń od energii udaru wysokiej prędkości w konstrukcjach kompozytowych wytworzonych metodą nawijania włókna na mokro. Przedmiotem badań było pięć warstwowych rur kompozytowych zaprojektowanych z użyciem metody tablicowej. Metoda ta posłużyła do wyboru trzech wzorów mozaikowych różniących się wartością reszty skoku nawijania oraz liczbą przeplotów, będących miejscami koncentracji naprężeń i znacząco wpływających na wytrzymałość kompozytu. Wzmocnienie kompozytu stanowił rowing szklany ze szkła typu E, materiałem osnowy była natomiast żywica epoksydowa. Udarność kompozytowych konstrukcji nawijanych badano w zakresie dużych prędkości 140 ÷ 170 m/s z użyciem impaktora w postaci stalowej, ulepszonej cieplnie kulki o masie 2,0 g wystrzeliwanej z działa gazowego. Liniowa zależność pól uszkodzeń od energii udaru dla rur kompozytowych wytworzonych przez nawijanie włókna na mokro we wcześniejszych badaniach potwierdzona dla laminatów poliestrowo-szklanych, została zaobserwowana jedynie dla jednego materiału.
Słowa kluczowe: Kompozytowe konstrukcje nawijane, uszkodzenia udarowe, udar balistyczny, metoda nawijania.